The 4th International Symposium on More Electric Aircraft Technology (MEA 2017)

8–9 November 2017

Transient simulation and analysis of wing electrothermal ice protection system

Li Peng, Kang Yuanli, Song Yupeng, He Xunan

Department of More electric systems, COMAC Beijing Aeronautical Science & Technology Research Institute, Beijing, People's Republic of China
E-mail: lipeng1@comac.com

Published in *The Journal of Engineering*; Received on 10th January 2018; Accepted on 17th January 2018

Abstract: The transient behaviour of electric heating and de-icing of the wing is studied by numerical method. The thermal convection coupling method based on the equivalent heat transfer coefficient and the boundary condition iteration is developed for the two designed schemes of the electric heating system. According to the surface temperature, the internal temperature, and the icing condition, the system transient performance is investigated. The purpose of this study is to establish the de-icing transient model of the wing ice protection system, simulate the transient de-icing process and form the method of performance estimation. The results under different working conditions show that the temperature distribution of the skin surface is not uniform, rather presents certain regularity. The rising rate of temperature decreases with the increase of the temperature. The trend is more obvious at lower ambient temperature, when the ambient temperature rises, the surface temperature rises rapidly in a short period. Scheme 2 has certain advantages in heating capability, while the hot knives structure of scheme 1 can narrow and split the icing area.

1 Introduction

Aircrafts often encounter ice weather conditions in flight. Icing on windward surfaces of different parts may cause different influence to aircrafts. As the key parts to lift the aircraft, wings' aerodynamic quality influences the performance of the aircraft to a maximum extent. The icing on the windward surface of the wing slats will result in the decreasing of aircraft's lift, the increasing of air resistance, thus the deterioration of aircraft handling and stability and other air quality, and cause disaster [1]. To ensure flight safety, reduce the occurrence of ice accidents, ice protection system are usually installed on the aircraft. There are a variety of ice protection methods. Among them, the electrothermal method is efficient, easy to control and power saving, thus is more commonly used in aircrafts [2]. When the electrothermal ice protection system works, the skin surface is heated, once the temperature rises above the melting point of the ice, the ice on the surface is melted to a thin liquid layer, and then the ice layer falls off the surface under aerodynamic and centrifugal force.

However, in the working process of electrothermal ice protection system, it is prone to meet with overflow ice, internal overheating, de-icing failure and other issues due to the design defects. So it is necessary to conduct a certain performance verification analysis to ensure the safety before actual uses. De-icing performance verification can be achieved through numerical simulation, ice wind tunnel test, flight test and other means. Numerical simulation is budget, time-saving to carry out tests under different conditions, and is efficient to predict the performance of the ice protection system under the entire flight envelope.

Foreign researchers have carried out a lot of researches on the numerical simulation of the electrothermal de-icing process. Stallabrass [3] established a mathematical model of the electrothermal de-icing plate for the first time, and studied the influence of the thickness ratio of the inner and outer insulating layers, and then the optimum thickness ratios of the inner and outer insulating layers were obtained. In 1987, Masiulaniec [4] created a two-dimensional (2D) model using the conformal-coordinate transformation method to convert the stratified de-icing structure of the leading edges of the propeller to the Cartesian coordinate system to overcome the problem of calculating curvature. Wright [5] carried out massive numerical simulations to investigate the de-icing process; the results showed that the alternating direction implicit (ADI) method was superior whose large time step did not cause divergence of the calculations. Yaslik established a 3D mathematical model of the simplified electrothermal de-icing device in 1992 [6]. In recent years, representative studies of electrothermal ice protection system have included: Elangovan and Olsen [7] established a mathematical model of the composite layer of the ice protection system by ADI method. Temperature field was obtained by solving the transient heat transfer equations, the control law was researched, and the number and position of the heating mat are optimised. Reid calculated the transient 2D de-icing process [8], and researched the impacts of icing, overflow water and structural model on the surface temperature by coupling the external icing and internal thermal conduction. Habashi simulated the 3D de-icing process, analysed the influence factors of de-icing effect by self-developed Fensap programme [9–11]. The optimisation method of the de-icing system is also studied.

Domestic research is relatively few due to the lack of the understanding of the importance of aircraft ice protection system and the complexity of the numerical calculation of electrothermal de-icing devices. In 1999, Han verified the performance of the anti-icing device on the radome for a certain aircraft [12]. Chang researched the thermal protection range of the ice protection system [13], which was installed on the propeller blade of a certain helicopter, and simulated the transient heat transfer process of the 2D electrothermal de-icing rectangle [14, 15]. Xiao calculated the thermodynamic coupling characteristics of the electrothermal de-icing process and its effect on de-icing performance, obtained the change regulation of the ice layer stress with the heat flux, and predicted the damaging effect of thermodynamics coupling on the ice [16].

In this paper, the electrothermal de-icing process of the wing is numerically studied. Aiming at the two schemes of the electric heating system, the method of internal heat conduction and external heat convection coupling is developed. On the basis of the change

of the surface temperature, interior temperature and icing conditions during the de-icing process, the performance of the system was investigated. The purpose of this paper is to establish the de-icing model of the wing ice protection system and simulate the transient de-icing process. The simulation includes the calculation of air flow field and the water droplet field, heat conductivity of internal layers of the composite heating mat, heat coupling of conductivity and convection, and mass transfer across the skin surface. Besides, the method of estimating the de-icing performance of the ice protection system is obtained, which can verify the rationality of the design scheme.

2 Mathematical model and calculation method

2.1 Electric heating device structure

The electrothermal device is installed inside the skin with an electric heating composite layer structure, which is usually composed of the corrosion protection layer (wear resistance layer), heating layer, adiabatic (inside and outside insulations) layer, support layer and so on. Figs. 1 and 2 show the two schemes of heating mat structure of electric heating device introduced in this paper.

As shown in Fig. 1, the heating mat of scheme 1 is mainly composed of metal heating element, glass fibre cloth and special glue. Glass fibre cloth is used for insulation, between the heating element and the outer skin; special glue is used to paste the heating element, the fibre cloth, the stainless skin, and the base layer by layer, and ensure the insulation between different layers as well. The stainless steel is corrosion resisting with high strength, so it can protect the entire heating device, besides, because of its high thermal conductivity, the anti-icing efficiency of the outer surface can be ensured.

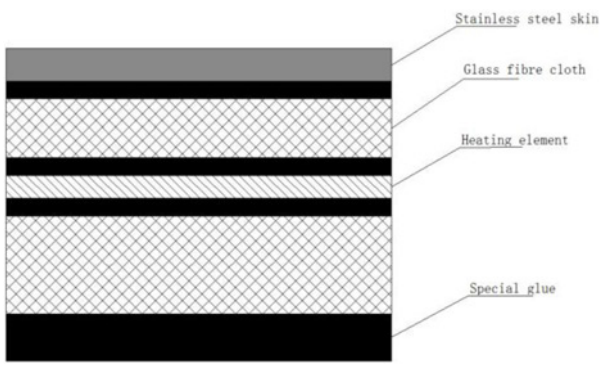

Fig. 1 *Heating mat structure of scheme 1*

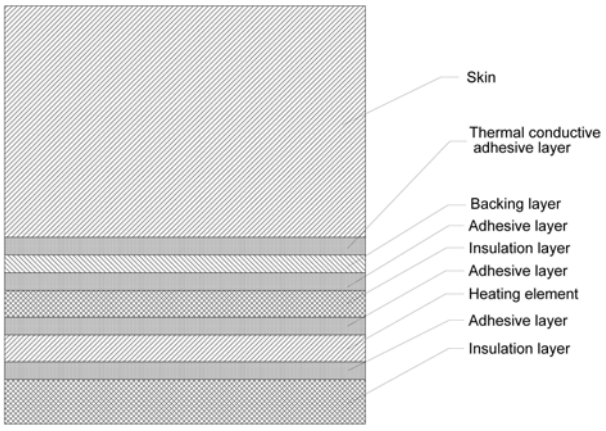

Fig. 2 *Heating mat structure of scheme 2*

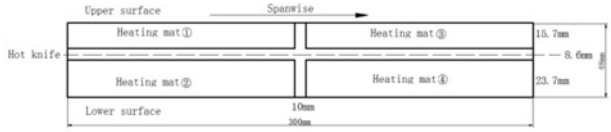

Fig. 3 *Heating scheme 1*

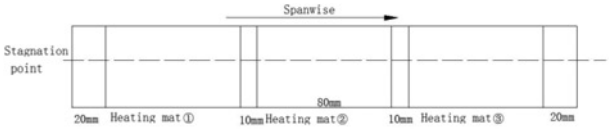

Fig. 4 *Scheme 2 structure*

The heating mat of scheme 2 is composed of skin, thermally conductive adhesive layer, backing layer, an adhesive layer, an insulation layer, heating layer and so on.

Meanwhile, the layout of the heating element is designed for scheme 1 and scheme 2. The heating element of scheme 1 uses the heating mat structure as shown in Fig. 1, and the heating element of scheme 2 uses the heating mat structure as shown in Fig. 2. The layout of the heating element as shown in Fig. 3 is designed for scheme 1, whereas the layout shown in Fig. 4 is designed for scheme 2.

For scheme 1, the chordwise width of the spanwise hot knife is 8.6 mm, the spanwise width of the chordwise hot knife is 10 mm, the cross-hot knife is symmetrical about the central line of the protected domain, and the area is 2974 mm^2, which accounts for 20.7% of the total area. The use of the cross-shaped hot knife can divide a large piece of ice into four small pieces, so they can be easily blown off from the skin when the ice at the interface is melted, thus the efficiency of de-icing is improved. When the temperature of the heating element is super high, the signal transmitted through the temperature sensor may cut off the power automatically to protect the heating elements.

For scheme 2, the heating elements ①, ② and ③ are installed in turn along spanwise. The size of the heating elements is the same, 80 mm in spanwise, and 40 mm in chordwise, the area of each element is 3840 mm^2.

The heat flux of scheme 1 and scheme 2 are both 2.8 W/cm^2, the heat flux of the cross-heat knife of scheme 1 is 2.05 W/cm^2.

2.2 Internal thermal simulation

The models are based on following hypotheses:

(1) The material properties of each layer of the heating mat are fixed.
(2) The interface between ice/water droplets and the skin surface, and each layer adheres perfectly.
(3) Ice block may fall off when the interface at the skin is melted. The melted thickness in this paper is supposed to be 0.2 mm.

The enthalpy equation of each layer of the heating mat is shown below:

$$\frac{\partial H_j}{\partial \tau} = k\left[\frac{\partial^2 t_j}{\partial x^2} + \frac{\partial^2 t_j}{\partial y^2} + \frac{\partial^2 t_j}{\partial y^2}\right] + q_j \quad (1)$$

where H is the total enthalpy (J) of the control volume; t is the temperature (K) of the control volume; k is the thermal conductivity (W/m k) of the control volume; j stands for appointed layer, q is internal heat source (W/m^2), the internal heat source of different layers equals 0 except the heating layer.

The enthalpy of the layers of the ice protection system presents a linear trend when the temperature rises, while that of the mixture of ice and water at the interface presents a non-linear trend because the temperature of the mixture is always fixed. In this paper, an improved enthalpy model is applied to analyse the heat transfer process of the mixture layer. It is assumed that the phase transition process takes place within a very small temperature range ($\Delta t = 0.02$°C). The relationship between the enthalpy of ice (water) and the temperature is shown as follows:

For ice layer ($t < t_m$)

$$H_i = \rho_i c_{\rho_i} t \tag{2}$$

For water layer ($t > t_m + \Delta t$)

$$H_{im} = \rho_i c_{p_i} t_m \tag{3}$$

$$H_{wm} = \rho_w (c_{p_i} t_m + L) \tag{4}$$

$$H_w = \rho_w c_w (t - t_m) + \rho_w (c_{pl} t_m + L) \tag{5}$$

For mixed layer($t_m \le t \le t_m + \Delta t$)

$$H_m = H_{im} + (t - t_m)(H_{wm} - H_{im})/\Delta t \tag{6}$$

where subscripts *i, m*, and *w* stand for ice, a mixture of ice and water, and water, respectively. ρ stands for density(kg/m^3); c stands for the specific heat at constant pressure (J/kg K). L stands for the latent heat of phase transition (J/kg) of ice. t_m stands for the phase transition temperature (K) of water. Δt is the temperature range of phase transition.

In the working process of electrothermal ice protection system, the heat transfer on the outer surface of the wing is various and complicated. Therefore, the concept of equivalent heat transfer coefficient h_{eff} is introduced in this paper, and the synthetic heat transfer process is simplified as $h_{\text{eff}}(t_s - t_\infty)$. Applying the skin surface temperature t_s and the equivalent heat transfer coefficient h_{gff} to the boundary condition formula (7) of the governing (1), the surface temperature field can be calculated by coupling the interior heat conduction and exterior complex heat convection. The boundary conditions of the control (1) are:

Exterior boundary

$$-k\frac{\partial t}{\partial y} = h_{\text{eff}}(t_s - t_\infty) \tag{7}$$

Interior boundary

$$\frac{\partial t}{\partial y} = 0 \tag{8}$$

Side boundary

$$\frac{\partial t}{\partial x} = 0 \tag{9}$$

where h_{eff} stands for the equivalent heat transfer coefficient of the skin surface and the environmental air flow (W/m^2 k), while the internal layers are taken as adiabatic, t_∞ stands for the ambient temperature (K).

2.3 External icing simulation

As part of the de-icing process is accompanied by icing phenomenon, it is needed to simulate the icing conditions on the skin surface. The calculation of icing is mainly composed of flow field calculation, water droplet impact characteristics and heat and mass coupling calculation.

The flow of fluid follows the mass, momentum and energy conservation equation. For the calculation of the flow field of an airfoil with and without icing, this paper chooses *S–A* equation as the turbulence model [16], and uses FLUENT software to discretise the control equations by the method of volume control, then the SIMPLE algorithm is applied to solve the discretised equations. In this paper, ICEM software is used to mesh the computational domain. The far field which is 15 times the chord length is meshed by the C-type structured grids, while the solid layers are meshed by BLOCK structured grids. After the independent analysis of the grids, the grids numbers of the far field and solid layers are confirmed. In this paper, the supercritical airfoil of SC0710 developed by National Aeronautics and Space Administration is adopted as the object of study, the chord length is 300 mm. The far-field pressure is set as the boundary condition for the entrance of the air-droplet field, the surface of the airfoil is assumed to be a non-slip wall, upper and lower boundaries of the calculated domain are taken as adiabatic, as shown in Figs. 5 and 6.

In the calculation of the water droplet field, Lagrangian algorithm rather than Euler method is applied to save more computational resources, because there is no need to couple the droplet field with the air field. The following equation of water droplets for icing issues is established:

$$\frac{\mathrm{d}^2\vec{x}_d}{\mathrm{d}t^2} + \frac{c_d \mathrm{Re}_w}{24}\frac{18\mu}{d^2\rho w}\frac{\mathrm{d}\vec{x}_d}{\mathrm{d}t} = \frac{\rho w - \rho a}{\rho_w}\vec{g} + \frac{c_d \mathrm{Re}_w}{24}\frac{18\mu}{d^2\rho w}\vec{u} \tag{10}$$

The initial conditions are

$$\vec{x}_d(0) = (x_0,\ y_0,\ z_0) \tag{11}$$

$$\left.\frac{\mathrm{d}\vec{x}_d}{\mathrm{d}t}\right|_{t=0} = \vec{V}_\infty \tag{12}$$

where C_d is the resistance coefficient, Re_w is Reynolds number of water droplets, μ is the air dynamic viscosity (Pa s), $\vec{V}_\infty$ is the velocity of the flow from far field (m/s), g is the acceleration of gravity (m/s^2), $\vec{x}_d$ is the displacement of droplet (m), $\boldsymbol{u}$ is the velocity of the water droplet, t is time (s), and subscript 0 stands for the initial

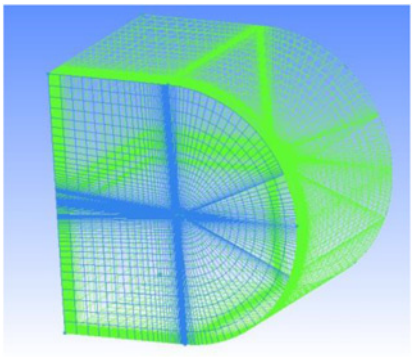

Fig. 5 *Wing far-field grid*

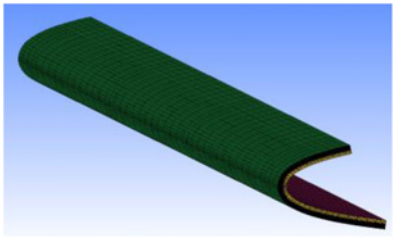

Fig. 6 *Solid grid*

conditions. On the basis of the classical Messinger icing model, the thermal and mass equilibrium of the icing process on the outer surface is studied. The specific solving process is introduced in literatures [17, 18].

2.4 *Calculation method of internal and external coupling*

Under icing conditions, the heat transfer process of the skin surface of the wing is complicated. Therefore, the concept of equivalent heat transfer coefficient h_{eff} is introduced in this paper, where the complex heat transfer process is simplified and expressed by formula (13), it can be seen that the internal heat conduction of the composite layers and the external heat convection are coupled to calculate the temperature field of the skin surface

$$Q = h_{\text{eff}} \Delta S (t_{\text{s}} - t_{\infty}) \tag{13}$$

where $Q = \Sigma Q_i(t_{\text{s}})$ is the sum of the heat flow (kW), t_{s} is the skin surface temperature (K), t_{∞} is the far-field temperature (K), and ΔS is the effective area of protection (m^2).

The coupling iteration follows these steps.

As shown in Fig. 7, the initial skin surface temperature is supposed to be t_{s}^0, then the updated surface temperature t_{s}^1, the equivalent heat transfer coefficient h_{eff}^0, and the thickness of the ice on the skin surface h^0 are calculated by the iteration of the external icing module. The internal heat conduction module is applied with t_{s}^1 and h_{eff}^0 set as the external boundary condition for the control volume. The 2D model is iterated after conformal transformation [5] to obtain the updated surface temperature t_{s}^2. t_{s}^2 is re-assigned to the external icing module, once the heat transfer and mass equilibrium are achieved, and the icing calculation is completed, the updated results of h_{eff}^1 and h^1 are obtained. According to the convergence criteria $|t_{\text{s}}^{k+1} - t_{\text{s}}^k| < \sigma$ (σ is a given constant), it can be determined whether the surface temperature is converged, if not, the process will be repeated. Then the surface temperature can be obtained for each timestep by carrying out the above steps.

3 Results and analysis

In this paper, the rationality of the design and the performance of the system are verified in the following aspects: the temperature field of the skin surface and its transient performance; the maximum temperature of the composite layers and its transient performance; the maximum icing thickness during the icing process and the characteristics of the de-icing process.

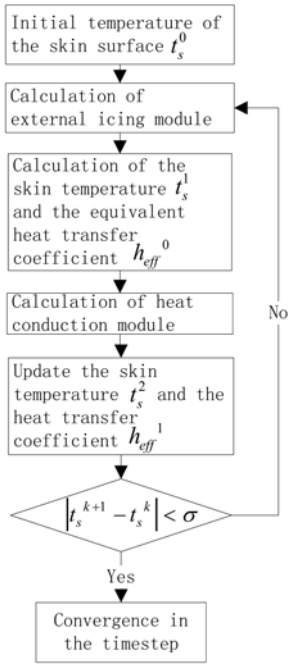

Fig. 7 *Iterative flowchart of internal and external coupling*

Table 1 Calculation conditions

Number	Altitude, km	Temperature, °C	Liquid water content (LWC), g/m^3	Velocity, m/s
1	2.5	−1.3	0.61	0.341
2	3	−4.5	0.54	0.369
3	3.05	−26	0.17	0.460
4	4	−11	0.4	0.426
5	5	−17.5	0.26	0.577
6	6.7	−28.6	0.15	0.657
7	4.6	−15	0.316	0.525

3.1 *Conditions for calculation*

According to the results of the thermal load obtained by empirical calculation, the working conditions of the larger thermal requirement in the flight envelope are selected. As shown in Table 1.

3.2 *Surface temperature field analysis*

As the temperature of the skin surface reaches the peak at the end of the heating cycle and declines to the lowest at the end of the cooling cycle, the analysis focuses on the surface temperature field at the end of the heating cycle and the cooling cycle.

Figs. 8 and 9 show the surface temperature distribution at the end of the heating cycle of scheme 1 and scheme 2 under the same working condition (case 6), respectively. As the water collection and the flow around the surface are different for the two schemes, the surface temperature distribution is not uniform but presents a

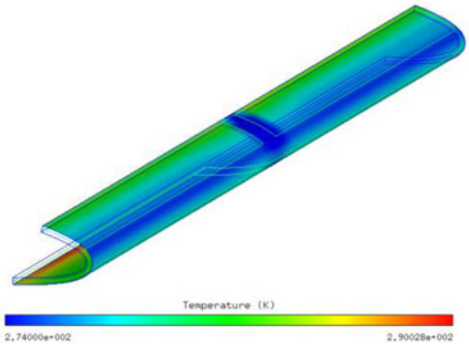

Fig. 8 *Surface temperature distribution of scheme 1 under working condition 6*

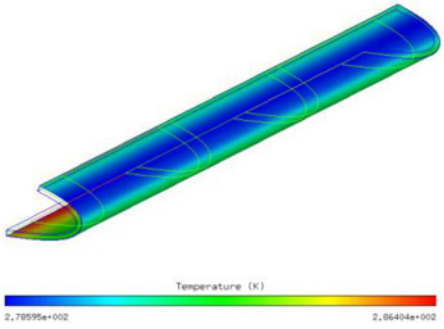

Fig. 9 *Surface temperature distribution of scheme 2 under working condition 6*

similar regular distribution. The maximum temperature of the surface of the two schemes is both located at the trailing edge of the lower surface, where the evaporation heat and the convection heat is rather low, due to the weak impact of the water droplets and the low velocity of air flow. The maximum temperature (17°C) of scheme 1 is larger than that of scheme 2 (13°C), because of the longer heating cycle. Since the heating power of the hot knife is lower than that of the heating mats on upper and lower surfaces for scheme 1, the surface temperature presents the same trend, as shown in Fig. 8.

The results show that the surface temperature range of the aircraft is different under different operating conditions in the flight envelope but present similar distribution regulations. The average temperature of the upper surface near the stagnation point is generally low because the water collection and the heat convection are enhanced. At the end of the heating cycle, the minimum temperature of the surface is between 5.5 and 10°C. Compared to other working conditions, the average temperature of case 6 is the lowest and the minimum temperature is 5.5°C. As shown in Table 1, the ambient temperature of case 6 is −28.6°C, the results demonstrate the availability of the schemes of the ice protection system.

During cooling cycle, case 3 and case 6 show typical frost situations, and the surface temperature is reduced to a minimum temperature of −5°C. The surface temperature of case 1 remains above 0°C due to the higher ambient temperature. For other calculated cases, the surface temperature drops to near 0°C, indicating that the interface at the surface is in the state of water/ice mixture.

The cross-shaped hot knife of scheme 1 is heated continuously, under conditions of case 3–case 7, the maximum temperature of the skin surface at the stagnation point is between 4.5 and 7°C, which is lower than 10°C.

3.3 Transient performance of the surface temperature

In the process of de-icing, the heating mats are heated periodically, thus the surface temperature fluctuates regularly. On the basis of the principle of heat and mass transfers, the impact of convective heat transfer on the upper surface at the downstream of the stagnation is much stronger than that on other protected area. Besides, comparing with the trailing region, the efficiency of water collection at the downstream of the stagnation is higher. Thus, it is generally taken as the key region to be investigated with the lowest surface temperature. This view is also proved by the results of the surface temperature distribution shown in Fig. 8. Temperature sensors are assigned to monitor the surface temperature, as shown in Fig. 10, the transient variation of the temperature of point ② is taken as emphasis.

Figs. 11 and 12 show the temperature changes of the sensor ② under different working conditions. It can be seen that the time needed for the heating cycle is different under different working conditions, so is the time needed for cooling cycle. The trend is the lower the ambient temperature, the longer the required heating time, and the shorter the allowable cooling time. After the heating element is powered, the surface temperature rises from the initial value, and the rate of rising decreases as the temperature increases. This trend is much more obvious while ambient temperature is lower (as cases 5, 6, and 7). When the ambient temperature is high, the surface temperature rises rapidly in a relatively short period of time (cases 2 and 4).

From the results of the calculations, it can be seen that the surface temperature of the monitoring point under the working conditions 1 and 2 is always >3°C and 1°C without freezing. While the surface temperature under the working conditions 2, 4, and 7 gradually decreases to 0°C and keeps stable, indicating that the interface on the surface is in the state of ice/water mixture.

Compared to scheme 2, the heating time required for scheme 1 is longer to reach a similar surface temperature. Taking case 7 as an example (as shown in Fig. 13), the heating time required for scheme 1 is 42.5 s, while the heating time required for scheme 2 is 32.5 s.

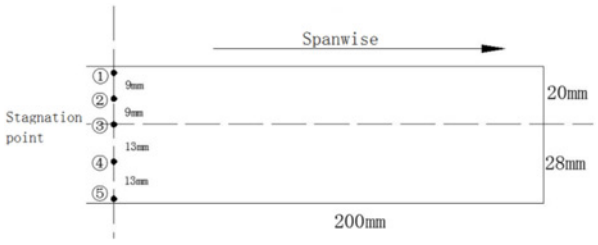

Fig. 10 *Temperature sensors distribution*

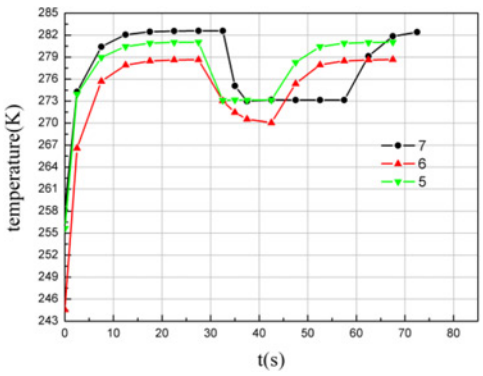

Fig. 11 *Temperature changes of sensor ② for scheme 2 under conditions of cases 5–7*

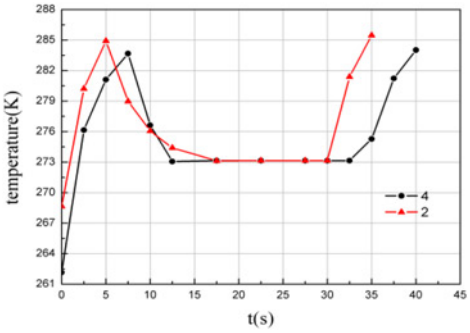

Fig. 12 *Temperature changes of sensor ② for scheme 2 under conditions of cases 2 and 4*

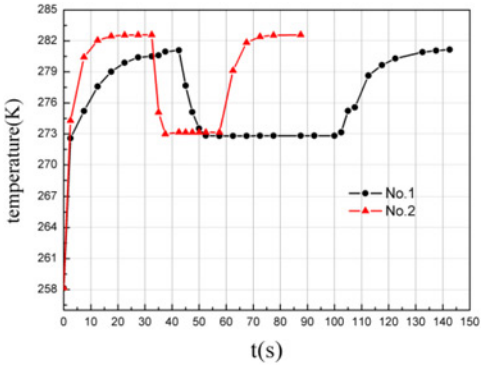

Fig. 13 *Comparison of temperature change for scheme 1 and scheme 2 on case 7*

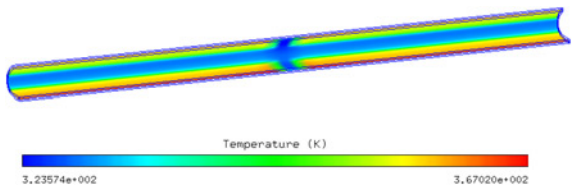

Fig. 14 *Temperature distribution of heating layer of scheme 1 under working condition of case 6*

3.4 Internal temperature of composite layers

During the de-icing process, the heating mats are periodically powered and the internal temperature of the composite layers therewith waves. The ice protection system limits the internal temperature to a certain extent by means of the temperature feedback. The purpose of simulating and investigating the internal temperature is to clarify whether the heating mat is overheated under the design working condition. Therefore, in order to prevent the material from overheating, the maximum temperature inside the heating mat during the de-icing process is investigated, that is, the temperature distribution at the end of the heating cycle.

Figs. 14 and 15 show the temperature profile of the heating layer of scheme 1, when the average temperature reaches the highest at the end of the heating cycle. The heating power of the cross knife is much smaller than that of the heating mat on the upper and lower surfaces, so the temperature of the hot knife is lower than other regions at the same moment during the heating cycle. Since the ambient temperature in case 6 is lower than that in case 7, the average temperature of the heating element of case 6 is lower, with a range of 50–94°C, while the range in case 7 is 55–98°C.

Figs. 16 and 17 show the temperature profile of the heating layer of scheme 2, when the average temperature reaches the highest at the end of the heating cycle. It can be seen that the temperature distribution of the internal heating element layer presents the similar characteristics to that of the skin surface, is affected by the ambient conditions. Owing to the lower ambient temperature of the working condition 6, the average temperature of the heating element layer is lower than that under the working condition 7. The temperature range of the former is 21–28°C, while the latter is 25–33°C.

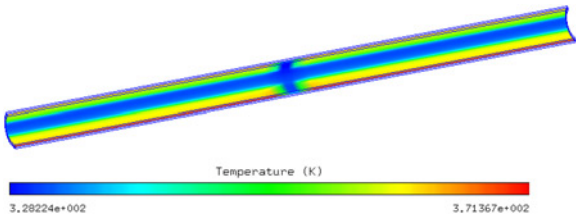

Fig. 15 *Temperature distribution of heating layer of scheme 1 under working condition of case 7*

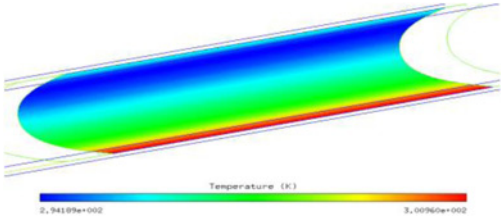

Fig. 16 *Temperature distribution of heating layer of scheme 2 under working condition of case 6*

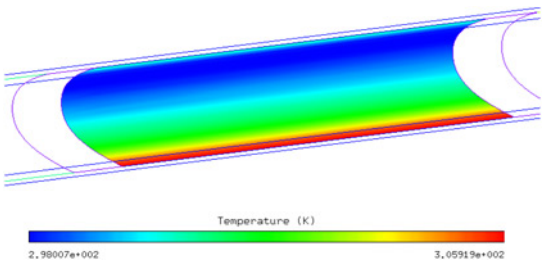

Fig. 17 *Temperature distribution of heating layer of scheme 2 under working condition of case 7*

The results of different cases show that the maximum temperature of the heating element layer of scheme 1 varies from 61 to 98°C. The maximum temperature of the heating element layer of scheme 2 varies from 20 to 33°C. Generally, the heat resistant temperature of the composite layers is higher than 120°C. Therefore, there is no overheating problem in the internal structure of scheme 2. Although the maximum temperature is much higher for the heating element of scheme 1 than scheme 2, the possibility of overheating is also tiny.

3.5 De-icing process

The ice protection system allows the skin to ice to a certain extent during the cooling cycle. This section examines the thickness of ice adhered to the protected surface at the end of cooling cycle, its severity is accessed and the de-icing characteristics are investigated.

Figs. 18–20 show the distribution of the icing thickness on the skin surface of scheme 2 under the working condition of case 7. The de-icing process of the system is revealed by the change

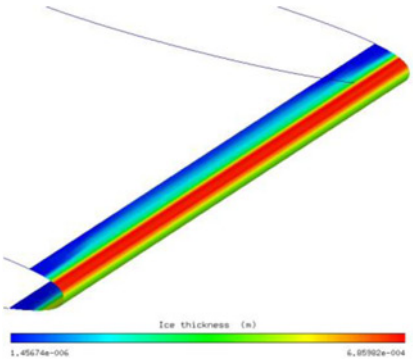

Fig. 18 *Icing thickness distribution sketch of scheme 2 in case 7 (57.5 s)*

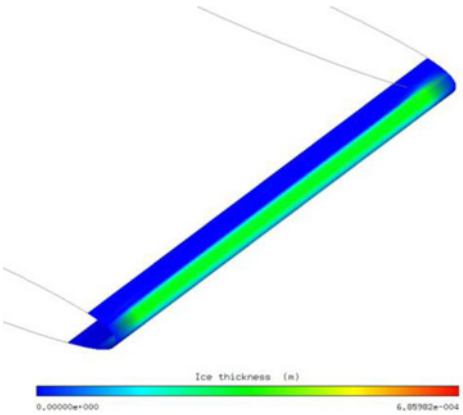

Fig. 19 *Icing thickness distribution sketch of scheme 2 in case 7 (60 s)*

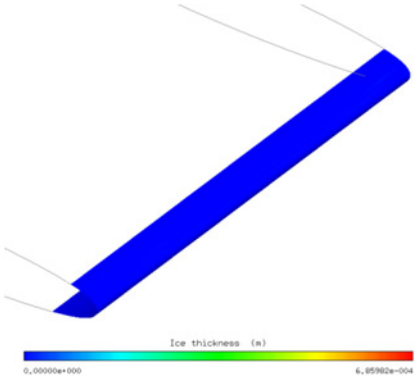

Fig. 20 *Icing thickness distribution sketch of scheme 2 in case 7 (62.5 s)*

of the cloud chart of the icing thickness with time. Fig. 21 shows the icing thickness distribution along chordwise at the cross-sectional position where $Z = 150$ mm, the abscissa is the coordinate value in the Y-direction, the unit is m, and the ordinate indicates the icing thickness, the unit is m.

The results show the transient de-icing process of the heating elements of scheme 2 under the working condition of case 7. It can be seen that the process of de-icing lasts in a short period of 5 s. From the end of the cooling cycle at 57.5–62.5 s, the maximum icing thickness on the skin surface decreases from 0.68 to 0 mm gradually, indicating that the ice adhered to the skin surface has been removed. It can be seen from Fig. 21, under the working condition of case 7, the ice presents the characteristics of glaze ice, where apparent ridges are formed on both sides of the stagnation point (see Fig. 22).

For the heating system of scheme 2, the surface temperature is always higher than 0°C due to the higher ambient temperature in case 1, so there is no icing occurring. The maximum icing thickness of the rest of the investigated cases is between 0.07 and 0.68 mm.

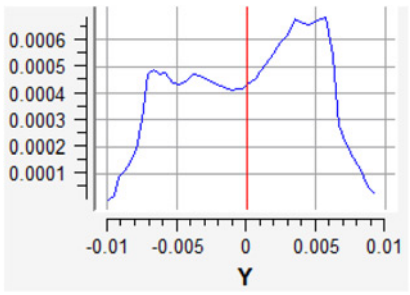

Fig. 21 *Icing thickness distribution ($z = 150$ mm) of scheme 2 in case 7 (57.5 s)*

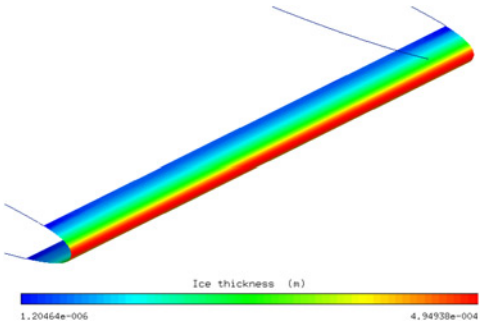

Fig. 22 *Icing thickness distribution sketch of scheme 2 in case 6 (47.5 s)*

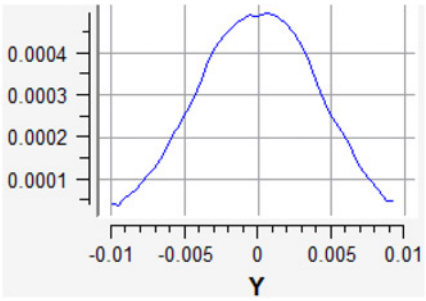

Fig. 23 *Icing thickness distribution ($z = 150$ mm) of scheme 2 in case 6 (47.5 s)*

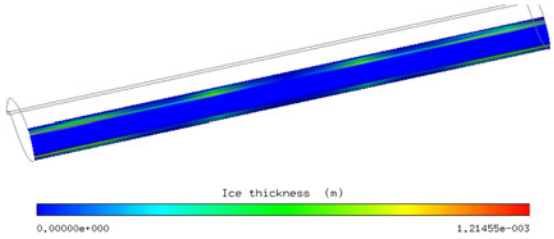

Fig. 24 *Icing thickness distribution sketch of scheme 1 in case 7 (62.5 s)*

Among them, apparent rime ice is generated in case 6 due to the lower ambient temperature, as shown in Fig. 23. According to the icing scale grades derived from flight test, the maximum icing thicknesses of 0.1–5 mm is taken as weak icing, which will not significantly affect the aerodynamic performance of the wing. Therefore, the control law of scheme 2 is safe and rational.

For the heating system of scheme 1, the surface temperature is always higher than 0°C due to the higher ambient temperature in case 1, so there is no icing that occurs too. The maximum icing thickness of the rest of the investigated cases is between 0.12 and 1.39 mm, which is also taken as weak icing. Meanwhile, throughout the de-icing process, there is no ice formed on the skin surface at the location of the hot knife area, as shown in Fig. 24. It is consistent with the design requirement of the system. The cross-shaped hot knife, whose surface temperature remains 6–10°C, is used to divide a large block of ice into small ones, so that they can be blown off from the skin surface by air flow easily.

4 Conclusion

In this paper, the problem of electrothermal ice protection system for the leading edge of wing slat is studied. According to the two specified heating schemes, the equivalent heat transfer coefficient and the internal and external coupling methods are used to calculate the temperature distribution of the skin surface. The effects of different working conditions on the surface temperature, internal temperature, and the transient de-icing process are studied.

A comprehensive evaluation of the simulation results is summarised as follows:

(1) Owing to the difference of water collection and outer flow, the temperature distribution of skin surface is not uniform, rather presents certain regularity. On the basis of the principle of heat and mass transfer, the impact of convective heat transfer on the upper surface at the downstream of the stagnation is much stronger than that on another protected area. Besides, comparing with the trailing region, the efficiency of water collection at the downstream of the stagnation is higher. Thus, it is generally taken as the key region to be investigated with the lowest surface temperature.

(2) During the de-icing process, the heating mats are periodically powered and the internal temperature of the composite layers therewith waves. The lower the ambient temperature, the longer the heating time required, and the shorter the permissible cooling time. The rate of temperature rising decreases as the temperature increases. This trend is much more obvious while ambient temperature is lower. When the ambient temperature is high, the surface temperature rises rapidly in a relatively short period of time.
(3) The structure and layout of the heating mat are different for the two specified schemes, so is the performance of the system. Overall, the surface temperature at the end of the heating cycle of scheme 2 is higher than that of scheme 1. In the meanwhile, the maximum temperature of the interior layers of scheme 2 ranges from 20 to 33°C, which is much lower than 61 to 98°C of scheme 1. Therefore, scheme 2 has the advantages to scheme 1 on heating performance. While the cross-shaped hot knife structure of scheme 1 can narrow and divide large ice blocks into small ones so that they can be blown away from the skin surface by air flow easily.

5 References

[1] Green S.D.: 'A study of U.S. inflight icing accidents and incidents'. pp. 1048–1073
[2] Qiu X., Han F.: 'Aircraft anti-icing system' (Aeronautic Specialty Textbook Read and Edit Group, Beijing, 1985), (in Chinese)
[3] Stallabrass J.R.: 'Thermal aspects of de-icer design'. Int. Helicopter Icing Conf., Ottawa, Canada, 23 May 1972
[4] Masiulaniec K.C.: 'A numerical simulation of the full two-dimensional electrothermal de-icer pad' (University of Toledo, Toledo, 1987)
[5] Wright W.B.: 'A comparison of numerical methods for the prediction of two-dimensional heat transfer in an electrothermal deicer pad' (University of Toledo, OH, Toledo, 1987)
[6] Yaslik A.D., DeWitt K.J., Keith T.G.: 'Further developments in three-dimensional numerical simulation of electrothermal deicing systems'. AIAA-92-0528, 1992
[7] Elangovan R., Olsen R.F.: 'Analysis of layered composite skin electro-thermal anti-icing system'. AIAA 2008-0446, 2008
[8] Reid T., Baruzzi G.S., Habashi W.G.: 'FENSAP-ICE: unsteady conjugate heat transfer simulation of electrothermal de-icing', *J. Aircraft*, 2012, **49**, (4), pp. 1101–1109
[9] Pourbagian M.: 'Power and design optimization of electro-thermal anti-icing systems via FENSAP-ICE'. AIAA 2012-2677, 2012
[10] Habashi W.G.: 'CFD-based optimization of electro-thermal wing ice protection systems in de-icing mode '. AIAA 2013-0654, 2013
[11] Habashi W.G.: 'On optimal design of electrothermal in-flight ice protection systems'. AIAA 2013-2937, 2013
[12] Han F., Chang S., Wang C.: 'Performance verification of aircraft radome anti-icing device', *Acta Aeronaut. Astronaut. Sin.*, 1999, **20**, (S1), pp. 87–89, (in Chinese)
[13] Chang S., Liu D., Yuan X.: 'Helicopter rotor blade anti/de-icing system protection scope study', *J. Aerosp. Power*, 2007, **22**, (3), pp. 360–364, (in Chinese)
[14] Chang S., Hou Y., Yuan X.: 'Effects of electric heating control law on the surface temperature', *J. Aerosp. Power*, 2007, **22**, (8), pp. 1247–1251, (in Chinese)
[15] Chang S., Ai S., Huo X.: 'Improved electrothermal de-icing system simulation', *J. Aerosp. Power*, 2007, **22**, (8), pp. 1247–1251, (in Chinese)
[16] Xiao C., Lin G., Gui Y., *ET AL.*: 'Thermal coupling characteristics of electrothermal de-icing and its effects on ice', *J. Exp. Fluid Mech.*, 2012, **26**, pp. 23–28, (in Chinese)
[17] Chi X., Li Y., Chen H.: 'A comparative study using CFD to predict iced airfoil aerodynamics'. AIAA 2005-1371.2005
[18] Yi X.: 'Numerical calculation of aircraft icing and icing scaling law' (China Aerodynamics Research and Development Center, Mian Yang, 2007), (in Chinese)